Contact resonance atomic force microscopy for viscoelastic characterization of polymer-based nanocomposites at variable temperature

Cite as: AIP Conference Proceedings **1749**, 020008 (2016); https://doi.org/10.1063/1.4954491
Published Online: 23 June 2016

Marco Natali, Daniele Passeri, Melania Reggente, Emanuela Tamburri, Maria Letizia Terranova, and Marco Rossi

Contact resonance atomic force microscopy for viscoelastic characterization of polymer-based nanocomposites at variable temperature

Marco Natali*, Daniele Passeri*, Melania Reggente*, Emanuela Tamburri†, Maria Letizia Terranova† and Marco Rossi*,**

*Department of Basic and Applied Sciences for Engineering, SAPIENZA University of Rome, Via A. Scarpa 16, 00161, Rome, Italy
†Department of Chemical Sciences and Technologies, University of Rome Tor Vergata and MinimaLab, Via della Ricerca Scientifica, 00133 Rome, Italy
**Research Center for Nanotechnology applied to Engineering of SAPIENZA University of Rome (CNIS), Piazzale A. Moro 5, 00185, Rome, Italy

Abstract. Characterization of mechanical properties at the nanometer scale at variable temperature is one of the main challenges in the development of polymer-based nanocomposites for application in high temperature environments. Contact resonance atomic force microscopy (CR-AFM) is a powerful technique to characterize viscoelastic properties of materials at the nanoscale. In this work, we demonstrate the capability of CR-AFM of characterizing viscoelastic properties (i.e., storage and loss moduli, as well as loss tangent) of polymer-based nanocomposites at variable temperature. CR-AFM is first illustrated on two polymeric reference samples, i.e., low-density polyethylene (LDPE) and polycarbonate (PC). Then, temperature-dependent viscoelastic properties (in terms of loss tangent) of a nanocomposite sample constituted by a epoxy resin reinforced with single-wall carbon nanotubes (SWCNTs) are investigated.

Keywords: Contact resonance atomic force microscopy; viscoelasticity; loss tangent; temperature; polymer; nanocomposite; carbon nanotubes;
PACS: 68.37.Ps; 68.47.Mn; 62.25.-g; 68.60.Bs; 81.05.Qk

INTRODUCTION

Reinforcement of polymers using suitable nanomaterials is a smart procedure to obtain nanocomposite materials with enhanced physical properties, including electric and/or thermal conductivity, strength, elasticity, toughness and durability, also in thermal management applications [1–3]. To set up reproducible synthetic routes, the properties of the obtained materials must be characterized from the macroscopic to the microscopic and sub-microscopic scale in the range of temperature of interest. As far as mechanical properties are concerned, dynamic mechanical analysis (DMA) is a well-established techniques which allows the independent measurement of the real and imaginary parts of the complex mechanical modulus of viscoelastic materials, i.e, the storage and loss modulus, respectively [4]. DMA can be performed at variable temperature, e.g., the so-called dynamic mechanical thermal analysis (DMTA), allowing for instance the identification of glass transition and other thermal transitions in polymeric materials [5]. Also, based on atomic force microscopy (AFM), counterparts of DMA have been developed which enable the characterization of viscoelastic materials at sub-micrometer and nanometer scale [6]. Due to its high spatial resolution, nanometer dimensions of the probed volume of materials, and nondestructive nature of measurements, AFM is currently a broadly used tool for the mechanical investigation of polymers community. AFM-based quasi-static nanoindentation is a well-established technique for the characterization of elastic properties of compliant materials [7, 8], also when they are represented by layered ultrathin films on stiff substrates [9, 10]. Also, it can be used to study viscoelasticity of soft materials through relaxation indentation tests [11]. Contact resonance AFM (CR-AFM) is a well-established but continuously evolving technique, in which the elastic modulus of samples is measured from the analysis of the flexural modes of the cantilever oscillating with the tip in contact with the sample surface [12, 13]. CR-AFM enables accurate measurement and mapping of elastic modulus in a broad range of values, e.g., from stiff crystals to polymers and biological materials [14, 15]. Also, CR-AFM characterization of elastic modulus of polymer blends at different temperatures was demonstrated [16]. Moreover, a recent improvement of CR-AFM, the so-called contact resonance AFM for viscoelasticity (CRAVE) [17, 18], has been recently improved to enable measurement and mapping of storage

NanoItaly 2015
AIP Conf. Proc. 1749, 020008-1–020008-8; doi: 10.1063/1.4954491
Published by AIP Publishing. 978-0-7354-1406-8/$30.00

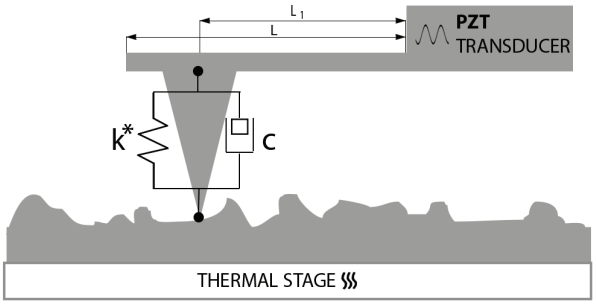

FIGURE 1. Sketch of the model used to analyze CR-AFM data.

and loss moduli as well as of loss tangent of viscoelastic materials [19–23]. Also, CR-AFM was recently demonstrated for the mapping of loss tangent of polymer blends at variable temperature from room temperature to about 80°C [24]. In this work, we describe the use of CR-AFM for the viscoleastic characterization of polymer-based nanocomposites at variable temperature. First, the method was demonstrated on two polymeric reference materials, i.e, low-density polyethylene (LDPE) and polycarbonate (PC), by studying the thermal dependence of their storage and loss moduli as well as of their loss tangent. Then, CR-AFM was demonstrated for polymeric nanocomposites by presenting a case study on epoxy resin loaded with single-wall carbon nanotubes (SWCNTs).

EXPERIMENTAL

Materials

A commercial blend of polystyrene (PS) and low-density polyethylene (LDPE) on Si substrate (PS/LDPE, Bruker Inc.) was used to assess the accuracy of the technique at room temperature [15, 25]. LDPE and polycarbonate (PC) sheets 1 mm thick (Goodfellow Cambridge Ltd.) were used as reference samples to verify the accuracy of CR-AFM for viscoelastic characterizations [26, 27]. LDPE and PC are characterized by different glass transition temperature, i.e., about -120°C and 140°C, respectively.

The case study was carried out on low viscosity epoxy resin formed by condensation between bisphenol A and epichlorhydrin, loaded with single-wall carbon nanotubes (SWCNTs) [28]. Triethylenetetramine was used as hardener, with a mixing ratio of 30:70 w/w. SWCNTs were produced by arc discharge and then purified in order to remove amorphous carbon and other residues. Nanocomposite sample was prepared by loading the epoxy resin with 3% in weight of SWCNTs, after dispersion of SWCNTs in $CHCl_3$ in ultrasonic bath with 9 runs of 1 h. The mixture was then further sonicated with ultrasonic bath and hand-stirring in order to optimize the dispersion. Finally, the corresponding weight fraction of hardener was added and the whole mixture has been dispersed again in an ultrasonic bath and hand-stirring for several minutes [28].

Experimental apparatus and equipment

Experiments have been performed using a standard AFM apparatus (Solver P47H, NT-MDT, Russia), in air and at room conditions. The samples are mounted on a heating stage (SU003, NT-MDT, Russia), consisting of a holder (15×17 mm^2), a temperature sensor (semiconducting diode), an a heating device (resistance) controlled by the AFM electronics with a voltage of 5 V and a maximum power of 4 W to reach a maximum temperature as high as 130°C. The sample and the holder were coupled using a Silver-based thermally conductive paste. Before carrying out CR-AFM measurements, we have to wait until the surface of the sample has reached the desired temperature to avoid thermal drift during the experiment. The time required for reaching the thermal equilibrium depends on the sample thermal conductivity and thickness. In case of LDPE and PC, thermal equilibrium was reached in 5 minutes, while the thicker epoxy and epoxy/SWCNTs required at least 10 minutes. CR-AFM experiments have been performed using commercial

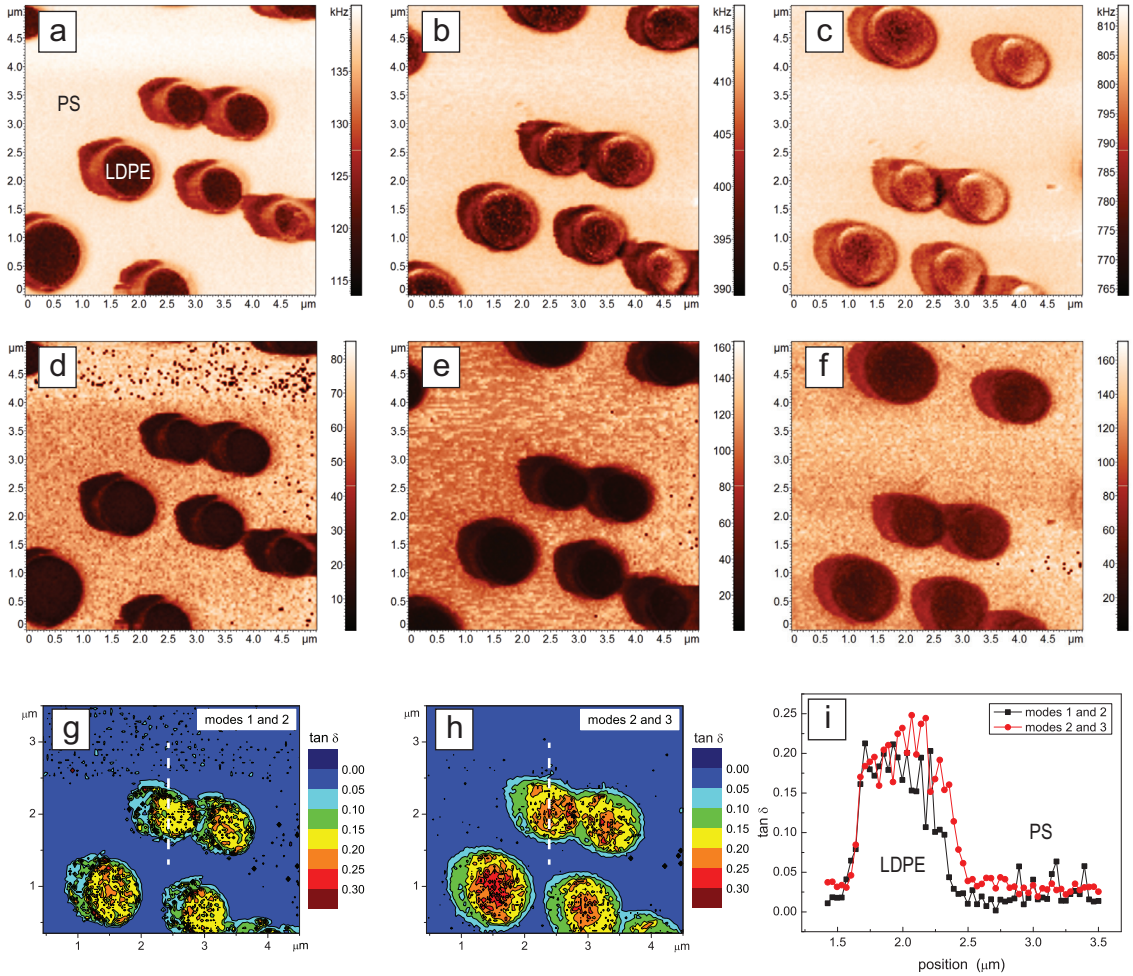

FIGURE 2. CR-AFM characterization of a reference LDPE/PS polymeric blend at room temperature. Maps of the contact resonance frequencies f_1 (a), f_2 (b), and f_3 (c), and maps of the corresponding quality factors Q_1 (d), Q_2 (e), and Q_3 (f). Maps of $\tan\delta$ obtained from the analysis of modes 1 and 2 (g) and of modes 2 and 3 (h). (i) Profiles of $\tan\delta$ values extracted in correspondence of the dotted lines in (g) and (h).

Si cantilevers (CSG-10, NT-MDT, Russia), with nominal dimensions: length L= 230 ± 5 μm, width w= 40 ± 3 μm and thickness t = 2 ± 0.5 μm. In the experimental configuration used in this work, the ultrasonic piezoelectric transducer is coupled with the cantilever chip [16]. During CR-AFM experiments, we noticed a significant reduction in the reproducibility of our results above 70°C, in correspondence of which we observed a dramatic lowering of the cantilever deflection signal, preventing the immediate re-use of the probe. This problem is due to the presence of the Au reflective layer on the cantilever back. As temperature increases, a deformation of the cantilever is expected due to the different thermal expansion coefficients of Si and Au, which brings the cantilever out from the focusing conditions. Furthermore, even after the subsequent cooling, the previous signal heating characteristics are no longer obtained, which is probably due to a delamination of the Au reflective layer.

TECHNIQUE

In the first step of CR-AFM experimental procedure, the oscillation spectrum of the cantilever free of oscillating in air is analyzed to determine some of its flexural modes. For the n-th selected mode, the free resonance frequency f_n^0 and the quality factor Q_n^0 are measured and used to determine some characteristic parameters of the cantilever [17, 18]. The AFM tip is then brought in contact with the sample surface. The cantilever-tip-sample system is set into oscillation, e.g., through piezoelectric actuator coupled with the back of the sample [29] or with the cantilever chip [30, 31], through Schottky barrier depletion-layer actuation [32], or through photothermal excitation [33]. The contact between the sample and the tip, the latter placed at distance L_1 from the cantilever chip being L the cantilever length, can be modeled as the parallel between a spring with elastic constant k^* and a dashpot of damping σ. These new boundary conditions determine the contact modes of the cantilever. From the analysis of the cantilever oscillation spectrum, the contact resonance frequency (CRF) f_n and the corresponding quality factor Q_n are measured for the n-th mode. These parameters are used to evaluate the normalized contact stiffness $\alpha = k^*/k_c$ and the normalized damping $\beta = \sigma\sqrt{L_1^2/(9EI\rho A)}$, where k_c is the spring constant, E the Young's modulus, I the area moment of inertia, ρ the density, and A the cross-sectional area of the cantilever [17, 18]. In particular, to evaluate the tip position expressed in terms of the ration $r = L_1/L$, the contact resonance frequencies corresponding to two different modes are measured (say f_n and f_m, with $n \neq m$). r is obtained as the value in correspondence of which the two CRFs give the same contact stiffness, $k^*(f_n, r) = k^*(f_m, r)$, neglecting the damping σ [34–36]. After calibration of the tip geometry and mechanical properties [37–39], knowledge of α and β allows one to evaluate the sample storage and loss moduli, E' and E'', respectively [19, 20]. Calibration procedure, however, is a source of uncertainty and is responsible for the lengthening of each measurement session. To avoid calibration, viscoelastic properties of the sample can be obtained in terms of the loss tangent $\tan\delta$ defined as

$$\tan\delta = \frac{E''}{E'} \quad . \tag{1}$$

From CR-AFM data, $\tan\delta$ can be calculated as

$$\tan\delta = (\lambda_n r)^2 \frac{\beta}{\alpha} \frac{f_n}{f_n^0} \quad , \tag{2}$$

where λ_n is the solution of the characteristic equation for free flexural vibrations of the cantilever $1 + \cos\lambda_n \cosh\lambda_n = 0$, which can be calculated as high as $\lambda_1 = 1.8751$, $\lambda_2 = 4.6941$, $\lambda_3 = 7.8548$ for the first, second, and third flexural mode, respectively [21, 23]. Eq. (2) allows one to determine $\tan\delta$ without the explicit calculation of E' and E'' and, thus, without calibration of the tip using reference materials.

RESULTS AND DISCUSSION

Validation on reference materials

In order to assess the accuracy of CR-AFM at room temperature, we characterized the PS/LDPE reference sample which is constituted by circular regions of LDPE randomly dispersed in the PS matrix. Having elastic modulus of about 100 MPa, LDPE is softer than PS which has elastic modulus of about 2 GPa [15, 40]. The maps of the resonance frequencies of the first three modes, i.e., f_1, f_2, and f_3, respectively, are shown in Fig. 2a , b, and c, respectively. The Q-factor maps of the same modes are shown in Fig. 2d, e, and f, respectively. From the frequency images of the first two modes, the map of r was obtained neglecting the damping. The maps of r, f_1, and Q_1 were then combined to numerically solving the (complex) characteristic equation of the system in Fig. 1. The maps of α and β were thus obtained (images not shown). Using Eq. (2), these were finally used to obtain the map of $\tan\delta$ relative to modes 1 and 2 reported in Fig. 2g. An analogous analysis of the images of the second and third modes allowed us to obtain the map of $\tan\delta$ relative to modes 2 and 3 reported in Fig. 2h. The values of $\tan\delta$ obtained for the two couples of modes are in good agreement with each other as shown by the superimposition of two representative profiles reported in Fig. 2i. The measured values of $\tan\delta$ on LDPE and PS are 0.19 ± 0.01 and 0.025 ± 0.005, in good agreement with data reported in literature [41–43].

To verify the effect of the choice of the analyzed couple of modes, on the same area of the sample In order to verify

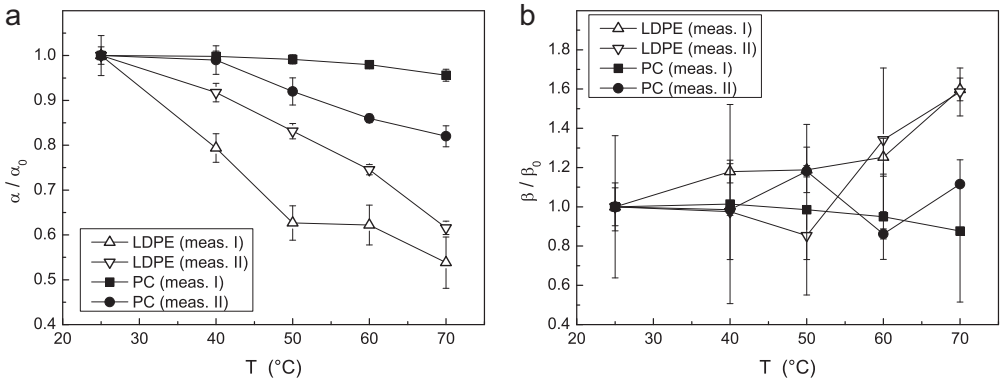

FIGURE 3. (a) Measured values of storage modulus E' normalized by its value at room temperature E'_0 as a function of the temperature T obtained in two different measurements on LDPE (open symbols) and PC (full symbols). (b) Measured values of loss modulus E'' normalized by its value at room temperature E''_0 as a function of the temperature T obtained in two different measurements on LDPE (open symbols) and PC (full symbols).

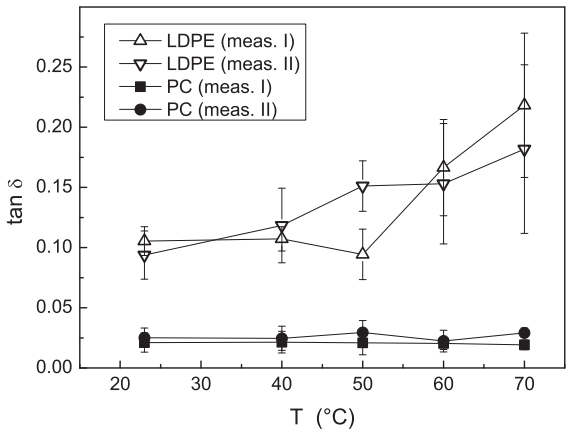

FIGURE 4. Measured values of $\tan\delta$ as a function of the temperature T obtained in two different measurements on LDPE (open symbols) and PC (full symbols).

the accuracy of CR-AFM for viscoelastic characterization at variable temperature, in the first part of this work two polymers with well-known mechanical properties (LDPE and PC) were studied. For each sample, each measurement session was performed using a different cantilever, the values of f_1^0, Q_1^0, and f_2^0 were preliminarily measured. At each temperature from 23°C to 70°C, f_1 and Q_1 were evaluated from statistics on maps, the size of which was chosen aiming at containing the time required for each measurement having nevertheless a statistically significant number of points, while f_2 was obtained by single point measurement in order to avoid excessive lengthening of the measurements session. Thus, f_1 and f_2 have been used to determine r by numerically solving the characteristic equation of the system depicted in Fig. 1 assuming $\sigma = 0$. The values of r we obtained were found to slightly vary among different measurements, doing range between 0.93 and 0.98. These values are in any case lower than the real value of $r = 0.985$ determined by scanning electron microscopy (SEM) images [25]. This can be attributed to the fact that lateral forces at the tip-sample contact increase the CRFs associated to each mode at relatively large values of k^*/k_c [44]. Neglecting these forces in CR-AFM data analysis results in 'effective' values of r smaller than the real one [39]. The determined values of r and the experimental values of f_1 and Q_1 were finally used to numerically solve the characteristic equation of the system in Fig. 1 in order to calculate α and β. Figure 3a shows the values of α normalized by the corresponding

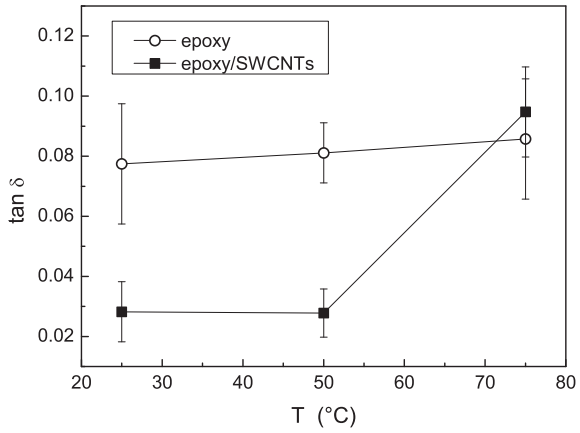

FIGURE 5. Experimental values of the loss tangent ($\tan\delta$) as a function of the temperature measured through CR-AFM on the epoxy (open symbols) and epoxy/SWCNTs (full symbols) samples.

value at room temperature α_0 obtained in two different experimental sessions on LDPE (open symbols) and in two different experimental sessions on PC (full symbols). α, which is proportional to the storage modulus E', is found to decrease on both the samples as temperature increases. In the case of PC, α is reduced to no less than 85% at 70°C, while more significant reductions to $55-60\%$ is observed in the case of LDPE. Figure 3b shows the values of β normalized by the corresponding value at room temperature β_0 obtained in two different experimental sessions on LDPE (open symbols) and in two different experimental sessions on PC (full symbols). In the case of PC, β (proportional to the loss modulus E'') is independent (within the experimental error) on temperature in the investigated range. Conversely, in the case of LDPE, β increases to 160% of its room temperature value at 70°C. The difference between PC and LDPE is more evident when the corresponding values of $\tan\delta$ (reported in Fig. 4) are considered. Indeed, in the case of PC, $\tan\delta$ is found to be independent on temperature, its mean value being 0.023 ± 0.004. The latter is in good agreement with the value of about 0.025, measured using DMA in the same range of temperature, recently reported in literature [45]. Conversely, $\tan\delta$ measured on LDPE definitely increases with temperature from 0.1 at room temperature to about 0.2 at $T=70$°C. These values are consistent with those (approximately from 0.13 to 0.23) obtained in the same range of temperature using DMA recently reported [41]. It should be explicitly noted, however, that the comparison among the results of mechanical characterizations obtained by different techniques on polymers reported in literature may be not significant and misleading. Indeed, mechanical properties of polymers may dramatically depend on the specific synthetic procedure and the aging of the material. Also, viscoelastic response is frequency dependent and thus a certain discrepancy may result from the different frequency ranges of CR-AFM and DMA [6, 46]. Finally, CR-AFM and DMA generally probe different volumes of sample under the surface. Thus, these techniques are differently affected by the presence of softer layers at the polymer surface [15]. Nevertheless, the results of the characterization of $\tan\delta$ of both PC and LDPE demonstrate the accuracy of CR-AFM technique for the viscoelastic characterization of polymer-based materials at variable temperature.

Case study: Epoxy/SWCNTs nanocomposites

In order to demonstrate the technique on polymer-based nanocomposites, we selected epoxy resin loaded with SWCNTs as a significant case study. The choice of this particular material is due to the scientific and technological interest in nanocomposites obtained by functionalization of polymeric matrices with Carbon-based nanomaterials, e.g., carbon nanotubes [47, 48] or nanodiamonds [49, 50]. The experimental procedure is the same we followed in the analysis of LDPE and PC, which is described above in details. Two different cantilevers were used to characterize the epoxy and the epoxy/SWCNTs samples, the values of f_1^0 and Q_1^0 of which are reported in Table 1. When in contact,

TABLE 1. CR-AFM experimental data obtained on epoxy and epoxy/SWCNTs samples. The parameters of the first mode of the free cantilevers (namely, the resonance frequency f_1^0 and the quality factor Q_1^0) are reported together with the corresponding ones with the tip in contact with the sample surface (namely, the contact resonance frequency f_1 and the quality factor Q_1) measured at three different temperature values.

			$T = 25°C$		$T = 50°C$		$T = 70°C$	
Sample	f_1^0 (kHz)	Q_1^0	f_1 (kHz)	Q_1	f_1 (kHz)	Q_1	f_1 (kHz)	Q_1
epoxy	27.5	55	141.8 ± 1.5	33 ± 1	139.2 ± 1.3	31 ± 1	137.2 ± 1.5	29 ± 1
epoxy/SWCNTs	24.5	88	138.5 ± 1.3	31 ± 1	137.5 ± 1.2	29 ± 1	134.5 ± 1.2	28 ± 1

values of f_1 and Q_1 were recorded for each sample on an area of $5 \times 1\ \mu m^2$, by applying a normal load of about 20 nN at three different temperatures, as reported in Table 1. As expected, for both the sample f_1 and Q_1 decrease as temperature increases f_1. The values of f_1 and Q_1 were used to calculate those of $\tan\delta$, which are shown in Fig. 5. The epoxy is characterized by a value of $\tan\delta$ of about 0.08, which seems to slightly increase but can be considered definitely constant in the investigated temperature range. From room temperature to 50°C, the epoxy/SWCNTs sample is characterized by $\tan\delta = 0.03$, lower than that of epoxy of more than 60%. At higher temperature, however, the value of $\tan\delta$ is the same of epoxy within the experimental uncertainty. This suggests that (at least in a region of the sample near the surface) at lower temperature the nanocomposite is actually reinforced by the presence of the SWCNTs fillers, while at high temperature its viscoelastic response is dominated by that of the epoxy matrix and the reinforcing effect of the nano-filler is lost.

CONCLUSIONS

CR-AFM is an AFM-base technique which allows one to characterize the elastic and viscoelastic response of materials at the nanometer scale at variable temperature. In this work, the potential of CR-AFM for the viscoelastic characterization of polymer-based nanocomposites has been demonstrated. First, the technique is illustrated on two polymeric reference materials, i.e., LDPE and PC. The analysis of the measured storage and loss moduli as well as of the loss tangent confirmed the accuracy of the technique. In particular, the loss tangent could be measured without any additional time-consuming calibration step. Then, a case study was presented in which CR-AFM was successfully employed in the characterization of a nanocomposite sample formed by epoxy resin reinforced with SWCNTs. CR-AFM measurements of $\tan\delta$ confirmed the reinforcement of surface of the material due to the presence of SWCNTs from room temperature to 50°C, while at higher temperature the viscoelastic response of the nanocomposite is mainly due to the epoxy matrix.

REFERENCES

1. C. Zweben, *JOM* **50**, 47–51 (1998).
2. H. Huang, C. H. Liu, Y. Wu, and S. Fan, *Adv. Mater.* **17**, 1652–656 (2005).
3. H. Liem, and H. S. Choy, *Solid State Commun.* **163**, 41–45 (2013).
4. C. C. White, M. R. Vanlandingham, P. L. Drzal, N. K. Chang, and S. H. Chang, *J. Polym. Sci. B Pol. Phys.* **43**, 1812–1824 (2005).
5. R. E. Wetton, R. D. L. Marsh, and J. G. Van-de-Velde, *Macromolecules* **175**, 1–11 (1991).
6. J. Le Rouzic, P. Delobelle, P. Vairac, and B. Cretin, *Eur. Phys. J. Appl. Phys.* **48**, 11201 (2009).
7. A. L. Weisenhorn, M. Khorsandi, S. Kasas, V. Gotzos, and H. J. Butt, *Nanotechnology* **4**, 106–113 (1993).
8. J. Domke, and M. Radmacher, *Langmuir* **14**, 3320–3325 (1998).
9. A. Kovalev, H. Shulha, M. Lemieux, N. Myshkin, and V. V. Tsukruk, *J. Mater. Res.* **19**, 716–728 (2004).
10. D. Passeri, A. Alippi, A. Bettucci, M. Rossi, A. Alippi, E. Tamburri, and M. L. Terranova, *Synth. Met.* **161**, 7–12 (2011).
11. S. Tripathy, and E. J. Berger, *J. Biomech. Eng. - T. ASME* **131**, 094507 (2009).
12. U. Rabe, J. Janser, and W. Arnold, *Rev. Sci. Instrum.* **67**, 3281–3293 (1996).
13. U. Rabe, M. Kopycinska-Müller, and S. Hirsekorn, "Atomic force acoustic microscopy," in *Acoustic scanning probe microscopy*, edited by F. Marinello, D. Passeri, and E. Savio, Springer-Verlag (Berlin, Heidelberg), 2012, chap. 5, pp. 123–153.
14. D. Passeri, A. Bettucci, and M. Rossi, *Anal. Bioanal. Chem.* **396**, 2769–2783 (2010).
15. D. Passeri, M. Rossi, E. Tamburri, and M. L. Terranova, *Anal. Bioanal. Chem.* **405**, 1463–1478 (2013).

16. F. Marinello, A. Pezzuolo, S. Carmignato, E. Savio, L. De Chiffre, L. Sartori, and R. Cavalli, *AIP Conf. Proc.* **1667**, 020009 (2015).
17. P. A. Yuya, D. C. Hurley, and J. A. Turner, *J. Appl. Phys.* **104**, 074916 (2008).
18. P. A. Yuya, D. C. Hurley, and J. A. Turner, *J. Appl. Phys.* **109**, 113528 (2011).
19. J. P. Killgore, D. G. Yablon, A. H. Tsou, A. Gannepalli, P. A. Yuya, J. A. Turner, R. Proksch, and D. C. Hurley, *Langmuir* **27**, 13983–13987 (2011).
20. D. G. Yablon, A. Gannepalli, R. Proksch, J. Killgore, D. C. Hurley, J. Grabowski, and A. H. Tsou, *Macromolecules* **45**, 4363–4370 (2012).
21. D. C. Hurley, S. E. Campbell, J. P. Killgore, L. M. Cox, and Yifu, *Macromolecules* **46**, 9396–9402 (2013).
22. D. G. Yablon, J. Grabowski, and I. Chakraborty, *Meas. Sci. Technol.* **25**, 055402 (2014).
23. A. B. Churnside, R. C. Tung, and J. P. Killgore, *Langmuir* **31**, 11143–11149 (2015).
24. I. Chakraborty, and D. G. Yablon, *Polymer* **55**, 1609–1612 (2014).
25. M. Reggente, M. Rossi, L. Angeloni, E. Tamburri, M. Lucci, I. Davoli, M. L. Terranova, and D. Passeri, *JOM* **67**, 849–857 (2015).
26. D. Passeri, A. Bettucci, A. Biagioni, M. Rossi, A. Alippi, M. Lucci, I. Davoli, and S. Berezina, *Rev. Sci. Instrum.* **79**, 066105 (2008).
27. D. Passeri, A. Bettucci, A. Biagioni, M. Rossi, A. Alippi, E. Tamburri, M. Lucci, I. Davoli, and S. Berezina, *Ultramicroscopy* **109**, 1417–1427 (2009).
28. D. Passeri, M. Rossi, A. Alippi, A. Bettucci, M. L. Terranova, E. Tamburri, and F. Toschi, *Physica E* **40**, 2419–2424 (2008).
29. D. Passeri, A. Bettucci, M. Germano, M. Rossi, A. Alippi, A. Fiori, E. Tamburri, M. L. Terranova, and J. J. Vlassak, *Microelectr. Eng.* **84**, 490–494 (2007).
30. K. Yamanaka, A. Noguchi, T. Tsuji, T. Koike, and T. Goto, *Surf. Interface Anal.* **27**, 600–606 (1999).
31. K. Yamanaka, and T. Tsuji, "Ultrasonic atomic force microscopy UAFM," in *Acoustic scanning probe microscopy*, edited by F. Marinello, D. Passeri, and E. Savio, Springer Berlin Heidelberg, 2012, chap. 6, pp. 155–187.
32. K. Schwarz, U. Rabe, S. Hirsekorn, and W. Arnold, *Appl. Phys. Lett.* **92**, 183105 (2008).
33. R. Wagner, and J. P. Killgore, *Appl. Phys. Lett.* **107**, 203111 (2015).
34. D. Passeri, A. Bettucci, M. Germano, M. Rossi, A. Alippi, S. Orlanducci, M. L. Terranova, and M. Ciavarella, *Rev. Sci. Instrum.* **76**, 093904 (2005).
35. D. Passeri, A. Bettucci, M. Germano, M. Rossi, A. Alippi, V. Sessa, A. Fiori, E. Tamburri, and M. L. Terranova, *Appl. Phys. Lett.* **88**, 121910 (2006).
36. D. Passeri, M. Rossi, A. Alippi, A. Bettucci, D. Manno, A. Serra, E. Filippo, M. Lucci, and I. Davoli, *Superlattices Microstruct.* **44**, 641–649 (2008).
37. G. Stan, and W. Price, *Rev. Sci. Instrum.* **77**, 103707 (2006).
38. F. Marinello, P. Schiavuta, S. Vezzù, A. Patelli, S. Carmignato, and E. Savio, *Wear* **271**, 534–538 (2011).
39. D. Passeri, M. Rossi, and J. J. Vlassak, *Ultramicroscopy* **128**, 32–41 (2013).
40. D. Passeri, A. Biagioni, M. Rossi, E. Tamburri, and M. L. Terranova, *Eur. Polym. J.* **49**, 991–998 (2013).
41. M. C. Guimarães Rocha, M. E. Leyva, and M. G. de Oliveira, *Polimeros* **24**, 23–29 (2014).
42. V. Mathur, K. S. Rathore, and K. Sharma, *World Journal of Nano Science and Engineering* **3** (2013).
43. A. Shojaei, and G. Li, *Proc. R. Soc. A* **470** (2014).
44. D. C. Hurley, and J. A. Turner, *J. Appl. Phys.* **102**, 033509 (2007).
45. A. S. Babal, R. Gupta, B. P. Singh, and S. R. Dhakate, *RSC Adv.* **5**, 43462–43472 (2015).
46. P. Vairac, J. Le Rouzic, P. Delobelle, and B. Cretin, "Scanning Microdeformation Microscopy: Advances in Quantitative Micro- and Nanometrology," in *Acoustic scanning probe microscopy*, edited by F. Marinello, D. Passeri, and E. Savio, Springer Berlin Heidelberg, 2012, chap. 8, pp. 227–259.
47. E. Tamburri, S. Orlanducci, M. L. Terranova, F. Valentini, G. Palleschi, A. Curulli, F. Brunetti, D. Passeri, A. Alippi, and M. Rossi, *Carbon* **43**, 1213–1221 (2005).
48. D. Sordi, S. Orlanducci, E. Tamburri, D. Passeri, M. Lucci, and M. L. Terranova, *Carbon* **43**, 2227–2234 (2011).
49. E. Tamburri, V. Guglielmotti, R. Matassa, S. Orlanducci, S. Gay, G. Reina, M. L. Terranova, D. Passeri, and M. Rossi, *J. Mater. Chem. C* **2**, 3703–3716 (2014).
50. D. Passeri, E. Tamburri, M. L. Terranova, and M. Rossi, *Nanoscale* **7**, 14358–14367 (2015).